Anomalously strong plasmon resonances in aluminium bronze by modification of the electronic density-of-states

N Shahcheraghi[1], V J Keast[2], A R Gentle[1], M D Arnold[1], and M B Cortie[1]

[1] *Institute for Nanoscale Technology, University of Technology Sydney, Broadway, NSW 2007, Australia*
[2] *School of Mathematical and Physical Sciences, University of Newcastle, Callaghan NSW 2308, Australia*

E-mail: Michael.cortie@uts.edu.au

Abstract

We use a combination of experimental measurements and density functional theory calculations to show that modification of the band structure of Cu by additions of Al causes an unexpected enhancement of the dielectric properties. The effect is optimized in alloys with Al contents between 10 and 15 at. % and would result in strong localized surface plasmon resonances at suitable wavelengths of light. This result is surprising as, in general, alloying of Cu increases its DC resistivity and would be expected to increase optical loss. The wavelengths for the plasmon resonances in the optimized alloy are significantly blue-shifted relative to those of pure Cu and provide a new material selection option for the range 2.2 to 2.8 eV.

Keywords: dielectric function, optical loss, copper-aluminium alloys, density functional theory (DFT), ellipsometry

(Some figures may appear in colour only in the online journal)

1. Introduction

Plasmonic phenomena are attracting considerable interest due to their many applications, including in biosensing [1, 2], metamaterials [3], spectrally-selective coatings [4, 5], or medicine [6, 7]. Excitation and propagation of a strong plasmon resonance in a material requires quite specific dielectric properties. If the dielectric function, ε, is expressed by

$$\varepsilon(\omega) = \varepsilon_1(\omega) + i.\varepsilon_2(\omega) \quad (1)$$

where ω is the frequency of light, then excitation of a plasmon requires that $\varepsilon_1 \leq 0$. In addition, the lowest practicable value of ε_2 is usually desired for plasmonic applications, while sharpness of the resonance peak is improved by maximizing $\frac{d\varepsilon_1}{d\omega}$ in the vicinity of the resonance. Furthermore, for practical reasons, materials used to develop plasmon resonances should be resistant to oxidation.

The alkali metals, especially Na and K, have excellent dielectric properties for these applications [8] but are too chemically reactive. In contrast, Ag and Au are nearly as good as Na or K but are expensive. The dielectric functions of Al and Cu are reasonably suitable for these applications [9] but these materials are not currently favoured because both are considered to oxidize too readily. In addition, the plasmon resonance of Al is at a relatively high energy while Cu is perceived to have a somewhat less attractive dielectric function. These latter issues can be partially compensated for by modifying the geometry of the plasmonic nanostructure (see Appendix).

The corrosion/oxidation problem in Cu can be ameliorated by surface passivation [10, 11], or by alloying with a second element, such as Al, that improves the oxidation resistance [12, 13]. Here we consider this last option, and explore the merits of (Cu,Al) α–phase alloys for applications that require a plasmonic response to light.

Of course, Cu-Al alloys are relatively cheap and non-toxic, but their DC resistivity is significantly higher than that of pure Cu and rises with increasing Al content. The greater resistivity is an indication that their optical applications are, in general, likely to be characterized by greater loss because the absorption coefficient, α, has a scattering contribution related to DC conductivity:

$$\alpha = \sqrt[2]{2\sigma_0\omega\mu_0} \quad (2)$$

where σ_0 is the DC conductivity and μ_0 the magnetic permeability of vacuum [14]. In addition, absorption due to interband transitions should also be considered when evaluating materials for plasmonics [15].

While ε_1 controls the frequency at which the LSPR occurs, ε_2 may be considered to primarily influence the quality of the resonance [8, 16]. Since the density-of-states of outer shell electrons controls the optical response of a metal [14, 17], it follows that a metallic material's dielectric function can be modified by changing its electron density [17, 18]. In terms of the Hume-Rothery rules, Cu is considered to possess a single valence electron whereas, in contrast, Al contributes three valence electrons per atom. Therefore, the electron density of Cu-base α-phase can be increased by substitutional alloying with Al and the dielectric function will be expected to change as a result. We speculated that the increased electron density imparted by Al additions would, overall, have a beneficial effect on the dielectric function and would enhance the intensity of selected plasmon resonances relative to those in a pure Cu structure. This intrinsic effect, however, would need to be carefully separated from the extrinsic effects due to nanoparticle geometry (Appendix, Figures A1 and A2).

2. Experimental

Copper and aluminium were co-deposited onto unheated glass substrates using a dual-target magnetron deposition system operating between 0.1 to 0.3 Pa (1×10^{-3} to 2×10^{-3} Torr). The substrates had been cleaned in solutions of detergent and acetone immediately prior to deposition. A quartz crystal microbalance was used to control the thickness of material deposited. Films were of the order of 1000 nm thick.

The as-deposited films were only weakly crystalline but were subsequently crystallized by annealing for 20 minutes at 770 K under an inert gas or vacuum environment. Sample structure and composition was assessed using a combination of X-ray diffraction (XRD) measurements and energy dispersive spectrometry (EDS). XRD was carried out on a Siemens D5000 X-ray diffractometer using Cu Kα radiation The lattice parameters of the samples were estimated from the {111}, {002} and {022} positions using Rietveld refinement. EDS was carried out using a Zeiss Evo Ls 15 SEM with a Bruker EDS Quantax 400 at 8 kV.

Reflectance, *R*, was measured between λ=300 nm and 2500 nm at 5 nm intervals using a Perkin-Elmer Lambda 950UV/VIS/NIR spectrophotometer with universal reflectance accessory at near normal incidence (8°). Ellipsometry measurement of the phase (ψ) and amplitude (Δ) of reflected waves) was carried out on a V-VASE Ellipsometer by J.A. Woollam Co. over the same spectral range and using angles of incidence of 65°, 70° and 75°.

The dielectric functions were extracted from the data using the WVASE 32 program of J.A. Woollam Co [13]. The dielectric functions were modelled as the sum of a Tauc-Lorentz oscillator [19, 20] (to simulate the absorption edge), two Lorentz oscillators (to account for additional interband transitions), and a Drude component (to model the low energy, intraband phenomena). It is likely that a very thin layer of Al_2O_3 will have been present on the surface of the samples but it had negligible impact on the optical properties as the ellipsometry fits were equally good for all three angles of incidence.

3. Calculations

The DFT calculations were performed using WIEN2K, an all-electron method that includes relativistic effects using the (linearized) augmented plane wave plus local orbitals method (LAPW+lo) method [21]. The generalized gradient approximation (GGA) of Perdew, Burke, and Ernzerhof (PBE) was used for the exchange-correlation potential [22]. The number of *k*-points was set sufficiently high (>50,000 for the smaller unit cells) that the resultant spectral details are not expected to change with more *k*-points. The maximum angular momentum for the radial wave functions (*lmax*) was chosen as 10 and the plane-wave cut-off (*RMTKmax*) was set to 7.0 The complex dielectric function was calculated using the random phase approximation (RPA) and neglecting local field effects (LFE) [23]. The RPA approximates the polarizability of the system as a sum over independent transitions. The momentum matrix elements are calculated from the electron states and an integration over the irreducible Brillioun zone is performed to calculate $\varepsilon_2(\omega)$. Finally, a Kramers–Kronig analysis is performed to obtain $\varepsilon_1(\omega)$. LFE are not expected to be significant in the low-energy spectral regions of interest here [24]. It is computationally convenient to split the calculations of the dielectric function due to inter- and intraband transitions into two separate calculations before summing them to obtain the final dielectric function. A broadening parameter of 0.1 eV was applied to the intraband Drude contributions for all of the systems. Further details about our methodology for the calculation of optical properties may be found elsewhere [25].

The addition of Al to Cu forms a disordered substitutional alloy, however the computational

method used here relies on a periodic crystal structure. To model a disordered crystal structure, a suitably sized fcc supercell was constructed and some of the Cu atoms replaced with Al. Our previous work on metal alloys has shown that the exact location of the substitutional atoms does not normally have a significant effect on the optical response [26, 27]. Additional tests on different atomic arrangements were performed here for the Cu-Al structures and the effect was similarly small, Figure 1. The lattice parameters were chosen based on literature data [28, 29].

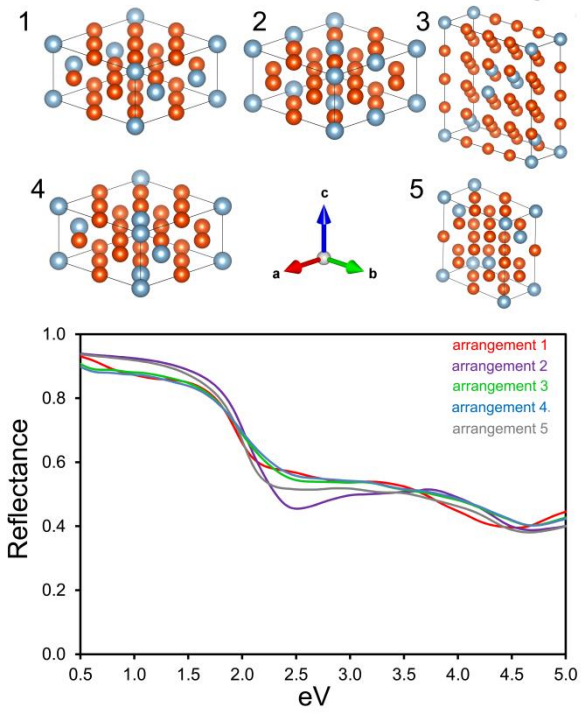

Figure 1. Effect of atomic arrangement on the calculated reflectance spectra of five variations of a material containing 18.75 at.% Al. The reflectance edge is at 2.00 eV ($2\sigma = \pm 0.06$ eV) in all cases.

The overall accuracy of the DFT calculations was checked by comparing the computed result for pure Cu to the measured dielectric function for that element, Figure 2. The prediction from the DFT calculation has the same shape as the measured data but places the absorption edge (defined here as the photon energy corresponding to the steepest part of the reflection edge) at about 1.67 eV (740 nm) rather than at the correct value of 2.20 eV (560 nm) [14]. This is a typical result for DFT which generally yields an absorption edge for coinage metals that is about 0.5 to 1.0 eV lower than the measured value [30-34]. The 'optical loss' (ε_2) of the calculated results is also about 2 units higher than the measured values. The literature data [30] for Cu and the data measured for Cu in our laboratory, define a scatter-band which can be used as a datum against which our later data for (Cu,Al) alloys will be compared.

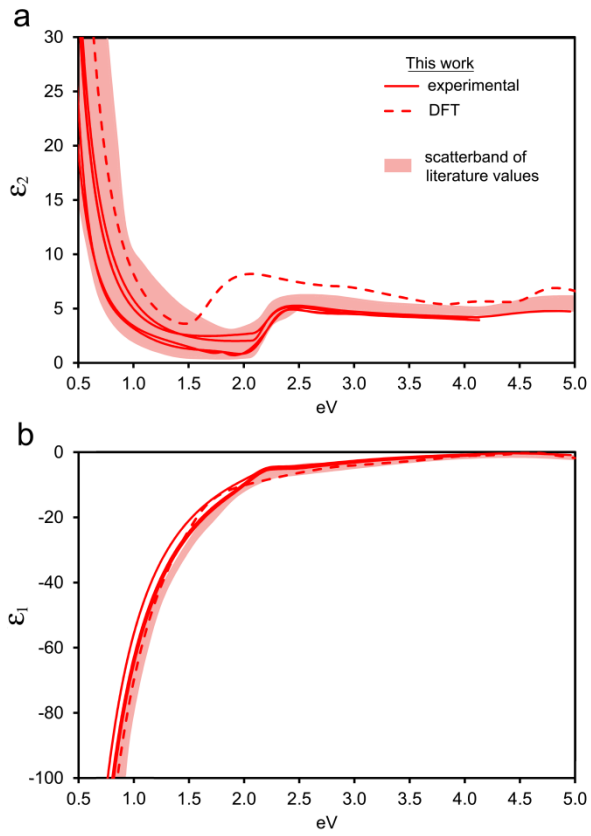

Figure 2. Scatterband of results for the dielectric function of pure Cu showing data taken from the present work (lines) and the literature (pink shaded region [17]), (a) ε_1, (b) ε_2.

The measured dielectric functions of the (Cu,Al) alloys were then used as input in electromagnetic simulations to provide a prediction of the strength of plasmon resonances in prototypical nanostructures. These simulations were conducted using the Discrete Dipole Approximation (DDA), implemented in the DDSCAT code of Draine and Flatau [35]. The target material is simulated by dipoles spaced at 1 nm intervals, a distance that is sufficiently close together to give numerical convergence in this case.

Statistical analysis of the data was performed with CurveExpert Professional (http://www.curveexpert.net).

4. RESULTS

After annealing, films containing up to ~19 at.% Al were found to consist of fcc α-phase, whilst samples with more than ~19 at.% Al were found to contain additional phases. This is in agreement with the equilibrium phase diagram [36] which shows that up to 19.6 at.% Al may be dissolved in Cu under room temperature equilibrium conditions with greater amounts leading to the formation of the Hume-Rothery electron compounds (β, γ, δ and ε). (These phases have optical properties that are quite distinct from those of (Cu,Al) α-phase and such samples

were discarded in the present study.) The atomic composition of the samples (as measured by EDS) was checked against an Al content estimated from the lattice parameter, a_0 (obtained from the XRD patterns, Figure 3). Literature data [28, 29] was used to establish the relationship between a_0 and Al%. Note that use of Vergard's Law alone would be unsatisfactory in this system as there is a significant negative deviation due to the strong Cu-Al bond [29]. A few samples showed a significant discrepancy (>2%) between the XRD-derived estimate for atomic % Al (which measured Al in the α-phase) and the EDS analysis (which measured total Al of all phases) and these outlying samples were discarded.

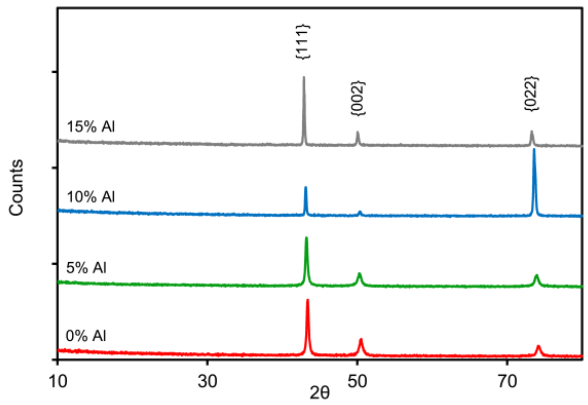

Figure 3. X-ray diffraction patterns of selected (Cu,Al) α-phase films. There is some crystallographic texture in the films and this causes a variation of relative peak heights.

Data for the calculated and measured dielectric functions of (Cu,Al) α-phase alloys, Figure 4, are in broad agreement: adding Al to Cu strengthens the interband transitions, blue-shifts the absorption edge and causes a monotonic increase in loss in the Drude region, Figure 5. The blue-shift in absorption edge is qualitatively explained in a rigid band model by the expectation that the addition of the extra valence electrons of Al fill the bands and increase the energy gap between the top of the *d*-band and the Fermi level. Blue-shifting of the lowest energy interband transitions decreases ε_2 at energies immediately above the absorption edge of Cu. In contrast, there is an increase in loss in the Drude region, which follows directly from the deleterious effect of Al additions on the DC electrical conductivity, as per Eq. 2. In general, this latter change would be disadvantageous in the context of sustaining a strong LSPR.

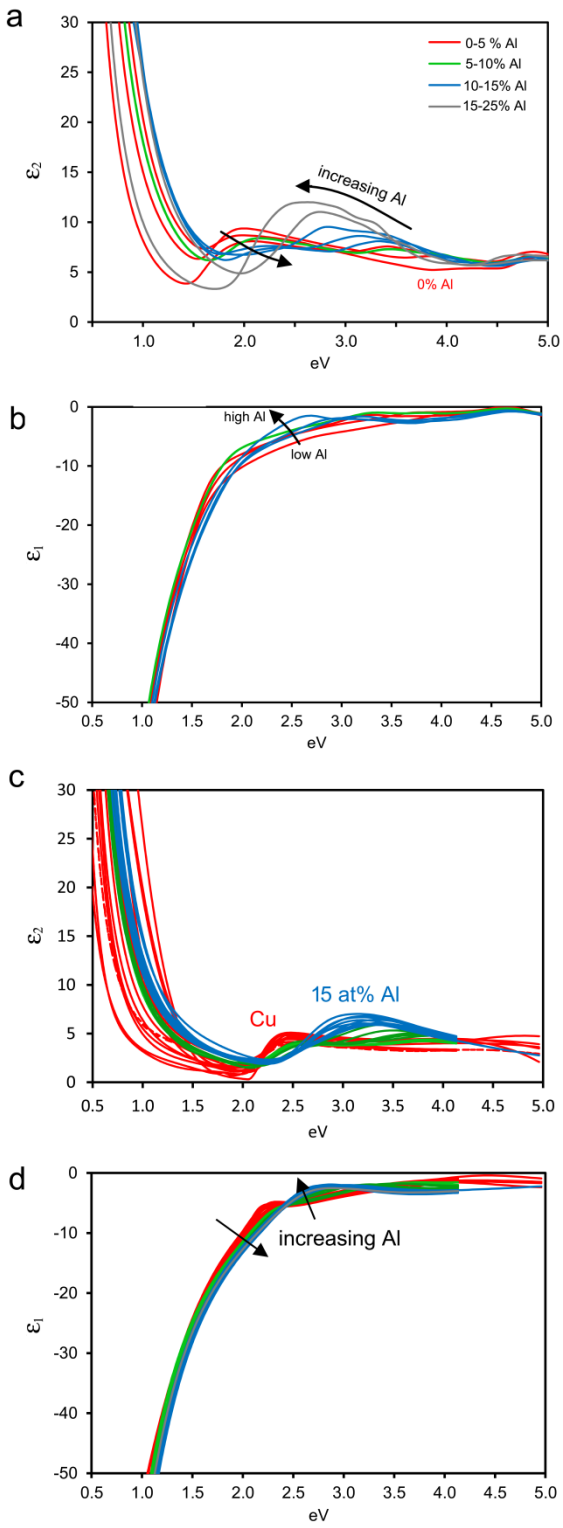

Figure 4. Dielectric functions of (Cu,Al) α-phase alloys, (a) and (b) calculated, (c) and (d) measured.

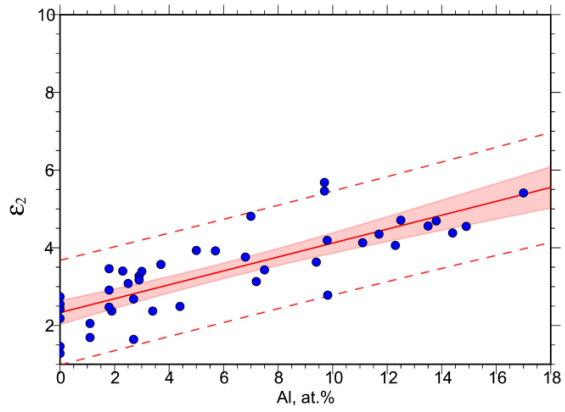

Figure 5. Effect of Al additions on the value of ε_2 in the Drude region of the spectrum, sampled here at 1.5 eV.

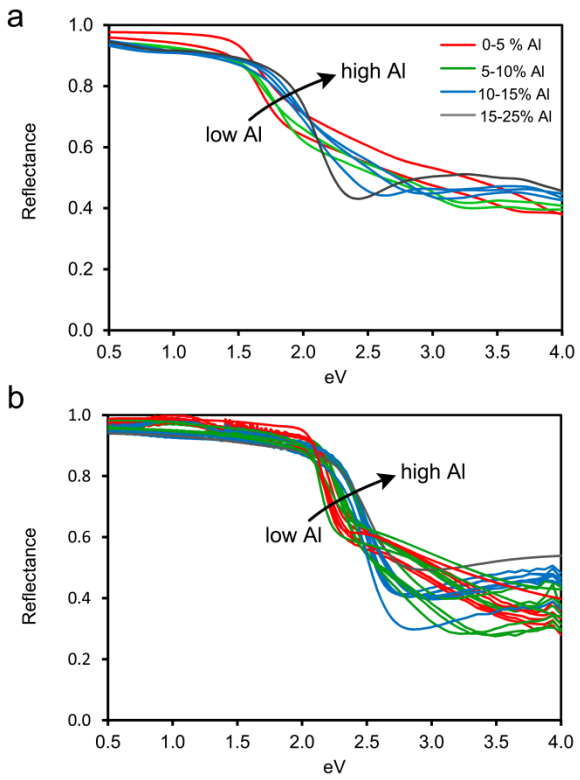

Figure 6. The effect of Al on the reflectance. (a) DFT calculation, (b) measured reflectance.

It is apparent that another effect of adding Al has been to increase ε_2 in the region between 3.0 to 4.0 eV. This causes a corresponding increase in reflectivity in that part of the spectrum, with the results of the DFT being in qualitative agreement with the measured reflectances, Figure 6. The shift in absorption edge seen in Figure 4a and 4c is similarly correlated with a shift in reflection edge, Figure 7a and 7b. The trend for both theoretical and experimental data is sigmoidal with little change up to 3 at.% Al and then a change of about 0.03 eV/at.% Al above that. The absence of an effect on the absorption edge in the dilute alloys has been attributed to screening of the Al-to-Al electronic interactions [37]. A similar blue-shift in the absorption edge due to increased electron density has been observed for Au-Cd alloys, and was noted to be beneficial for obtaining stronger plasmon resonances [18].

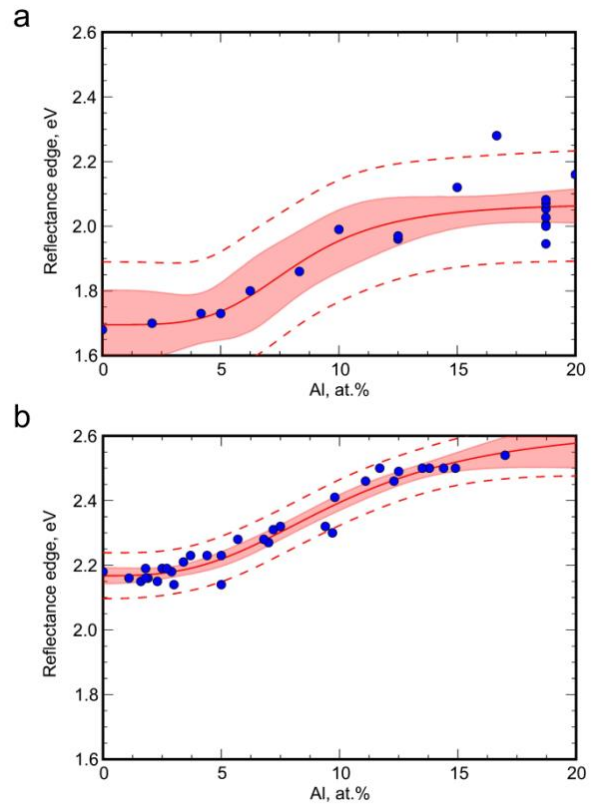

Figure 7. Position of reflectance edge as function of Al. (a) DFT calculations, (b) experimental data. Empirical models, associated 95% confidence intervals (shaded) and 95% prediction intervals (dashed) are superimposed on the data to guide the eye.

3. DISCUSSION

The effects of the interband transitions are evident as localized positive perturbations superimposed on the overall trends of ε_1 or ε_2 *vs*. frequency [18, 38]. The important issue here, however, is the role that this factor has on the strength and position of the LSPRs, Figure 8. The effect is revealed in a plot of the extinction efficiency Q_{ext} calculated for 20 nm diameter nanoparticles in vacuum.

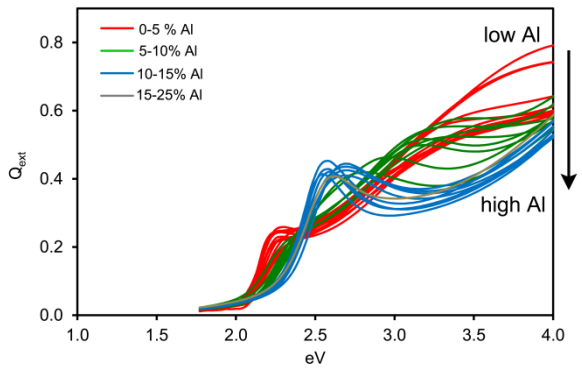

Figure 8. Effect of Al content on the optical extinction efficiency of a 20 nm diameter nanosphere of the indicated material, suspended in vacuum.

It is clear that adding Al will result in a considerable increase in the strength of a nanosphere LSPR and a simultaneous blue-shift of about 0.4 eV. The change seems optimized for Al content in the range of 13 to 15% at.% Al. Importantly, the LSPR is optimized and shifted towards the blue end of the visible range, a technologically useful region of the spectrum that is inaccessible to LSPRs in pure Cu or Au.

For pure Cu, a band analysis shows that the peaks in ε_2 between 2.2 and ~6 eV can be attributed primarily to transitions from the *d*-band to states above the Fermi level with the band edge onset at 2.2 eV due to transition from the top of this *d*-band. There is a minor contribution due to transitions from states just below the Fermi level to band that starts about ~4 eV above the Fermi level. When Al is added to the system, the d-band narrows slightly with the states at the top of band shifting to lower energy, and the band-edge onset in the spectra consequently moving up in energy, Figure 9. Similarly, the band at ~4 eV above the Fermi level, also moves down in energy and the previously minor contribution of transitions to this band now become a more significant contribution and are lower in energy. The changes in the interband transitions, revealed in ε_2, also change the shape of ε_1, because of the Kramers-Kronig relationship, making the LSPR more accessible to excitation at some frequencies.

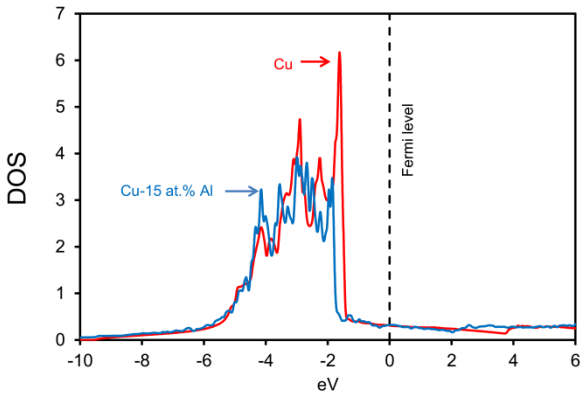

Figure 9. Calculated density of states of pure Cu and a Cu-15 at.% Al alloy, showing how the *d*-band is narrowed and moved up in energy by Al.

The enhancement in LSPR can be further improved by tuning the nanoparticle shape to match the optimum dielectric function. In Fig. 10a we show how this can be achieved using a series of nanorods of the 15 at.% Al alloy, each of the same volume (a_{eff} = 40 nm) but with a variable aspect ratio. As the aspect ratio is increased, the LSPR in the rod will be red-shifted and become stronger, however, there is a critical range of energies over which the optimum shape of nanorod made from the 15% at. % Al alloy will sustain a much stronger LSPR than corresponding rods made of pure Cu, Fig. 10b (see also animation in Supplementary Material). In contrast, there is no enhancement at photon energies of less than 2.15 eV, indeed, at these lower energies the result will be a 20% attenuation of the strength of the LSPR, Fig. 10c. This latter effect is mundane and follows from the known deleterious effect of Al on electrical conductivity in the Drude region. When the extinction efficiency is normalized relative to that of a pure Cu nanorod of the same aspect ratio, then it can be seen that a two-fold enhancement has been achieved over the optimum range, Fig. 10d. It is clear that the LSPRs in the 15% Al alloy have been enhanced by the alterations in dielectric function, principally by the reduction in the ε_2 of the alloy, relative to pure Cu, over the critical region of the spectrum in which the LSPR occurs.

The result is so striking that we believe the ~15 at.% 'aluminium bronze' alloy will have widespread utility in plasmonic devices. Therefore we suggest that it deserves a name of its own and propose 'orichalcum'. Orichalcum was a mythical and energy-rich noble metal alloy mentioned in Classical texts and its adoption for the modern low-loss alloy seems appropriate. For convenience, a representative dielectric function of orichalcum is provided here as Figure 11 and Table 1.

5. CONCLUSIONS

In summary, the dielectric function of (Cu,Al) α-phase can be modified by the increased electron density imparted by additions of up ~18 at. % Al. Addition of Al causes an increase in the optical loss in the Drude region but also blue-shifts the interband transition responsible for the reflectance edge of the alloy. This has the net effect of actually reducing ε_2 between 2.2 and 2.8eV (between 440 and 560 nm). Numerical simulations show that the strengths of localized surface plasmons located in this region of the spectrum are strongly increased relative to those on a pure Cu nanostructure. This surprising result is likely to provide at least two benefits: a mechanism to significantly improve the quality of localized surface plasmon resonances in a copper-base alloy and a strategy to blue-shift the resonances into the mid-visible (a region of the spectrum where pure Cu or Au are unsuitable).

Acknowledgments

We thank J.W. Wallace and C.J. Wrightson for performing preliminary DFT calculations, and Mr Geoff McCredie and Dr Sujeewa de Silva for assistance with experimental issues. This work was supported by the Discovery Program of the Australian Research Council.

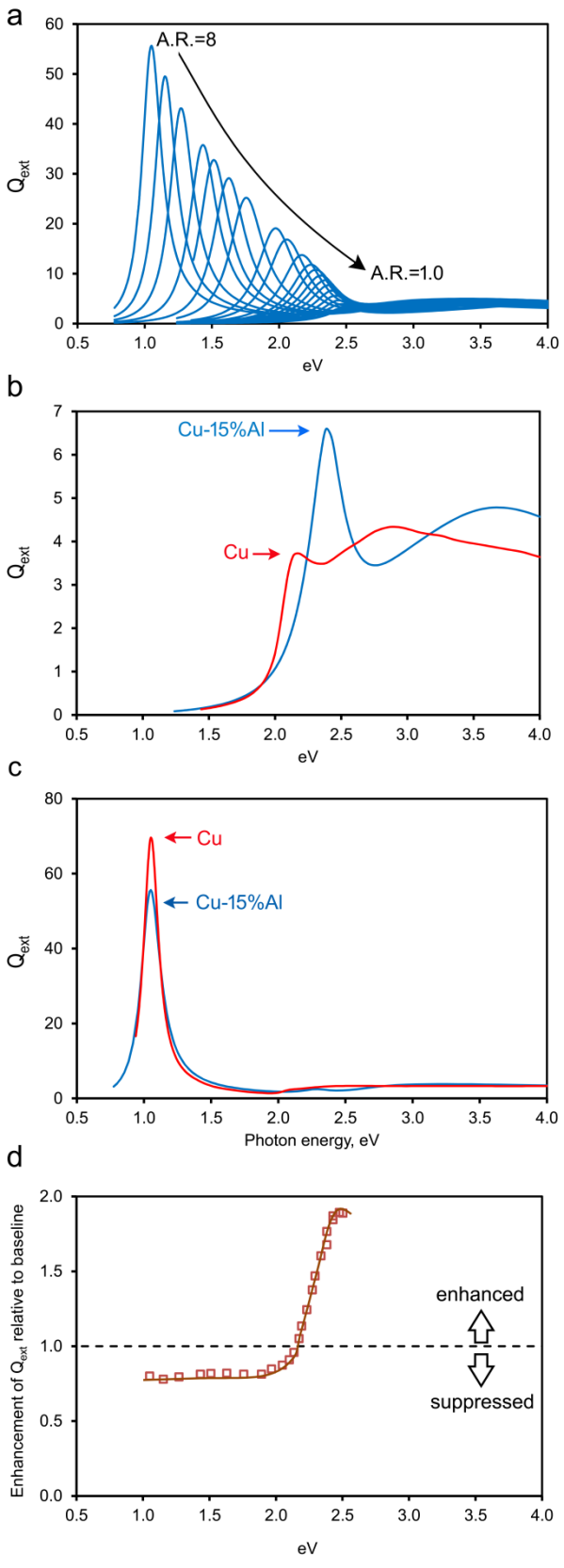

Figure 10. Optimization of LSPRs in 'orichalcum' alloy using alloy nanorods of constant volume but variable aspect ratio. (a) Q_{ext} for a series of equivolume nanorods of aspect ratio varying from 8 to 1. (b) Q_{ext} for nanorod of 1.5:1 aspect ratio compared to that of Cu rod of same dimensions. (c) Q_{ext} for nanorod of 8:1 aspect ratio compared to that of Cu rod of same dimensions. (d) Enhancement factor of Q_{ext} due to modification of dielectric function.

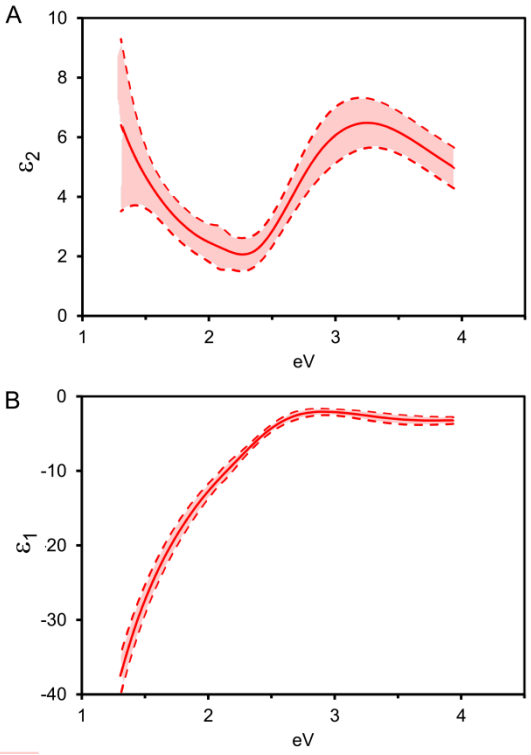

Figure 11. Dielectric function of Cu-15 at.% Al alloy ('orichalcum') produced by regression of the experimental data at each wavelength, followed by interpolation to yield estimates at 15 at.% Al. The 95% prediction interval is shown as dashed lines. (a) ε_2, (b) ε_1.

TABLE 1. Dielectric function of Cu-15.0 at.% Al

eV	ε_1	ε_2
1.3	-37.81	6.46
1.5	-27.28	4.63
1.6	-23.39	3.98
1.7	-20.12	3.45
1.8	-17.30	3.02
1.9	-14.86	2.69
2.0	-12.72	2.45
2.1	-10.83	2.26
2.2	-9.06	2.09
2.3	-7.33	2.07
2.4	-5.68	2.32
2.5	-4.29	2.87
2.6	-3.24	3.59
2.7	-2.55	4.36
2.8	-2.20	5.08
2.9	-2.09	5.65
3.0	-2.15	6.07
3.1	-2.30	6.33
3.2	-2.50	6.46
3.3	-2.72	6.46
3.4	-2.92	6.35
3.5	-3.09	6.15
3.6	-3.21	5.90
3.8	-3.28	5.34
4.0	-3.20	4.80

APPENDIX. GEOMETRIC OPTIMIZATION OF PLASMON RESONANCES IN PURE Cu

The optical properties of Cu, and its face centered cubic alloy with Al, have been quite extensively studied in the past [14, 33, 37-40]. Pure Cu has a unique orange-red colour caused by an absorption edge at about 2.2 eV (560 nm) [14]. This arises from the characteristic energies of the electronic transitions (the 'interband transitions') from the top of Cu's *d*-band to the half-filled 4s band at the Fermi level [38], which collectively absorb photons of energies of greater than about 2 eV. Hence, although a localized surface plasmon resonance (LSPR) occurs in pure Cu nanospheres at about 2.3 eV, it is relatively weak [10, 41] due to the high value of ε_2 (about 6 units) at this photon energy.

Stronger LSPRs in Cu can be obtained by increasing the aspect ratio of the nanoparticle undergoing resonance. This geometric change red-shifts the resonance frequency into a region of the spectrum where the ε_2 values for Cu are smaller. Due to these factors, most reports of LSPRs in Cu are for *non-spherical* nanoparticles [10, 42, 43]. Two effects are convoluted in this change in LSPR intensity: a purely geometric effect which always gives a stronger extinction efficiency for rods or ellipsoids anyway, and the effect of the reduced ε_2 due to the photon energy being red-shifted below that of the material's interband transitions [16, 44].

The extrinsic geometric effect can be separated from the intrinsic material effect by running a *gedankenexperiment* in which the LSPRs of the Cu nanorods are baselined against those of a hypothetical material in which ε_1 is the same as for Cu but in which ε_2 is set at 6.00 for all photon energies. This latter value is chosen because it is similar to that applicable for the case of LSPRs in Cu nanospheres, our baseline case. It should be noted that such a dielectric function would be forbidden by nature as it would not satisfy the Kramers-Kronig relations and thus violate causality. Nevertheless it provides a useful conceptual tool for the separation of the geometric effects.

These phenomena are illustrated in Figure A1 in which it is clear that the Q_{ext} of the LSPR but not its photon energy are affected by the changed dielectric function of the *gedankenexperiment*. Baselining the Q_{ext} of the Cu nanorods against that of the material of the *gedankenexperiment* permits the isolation of the effect of ε_2 in pure Cu, Figure A2. It can be seen the enhancement of optical extinction in pure Cu is maximized at a rod aspect ratio of about 2.5. The volume of each nanoparticle in these simulations is fixed at 268000 nm^3 (ie. an effective radius [35], a_{eff}, of 40 nm) so there is no variation due to amount of material involved.

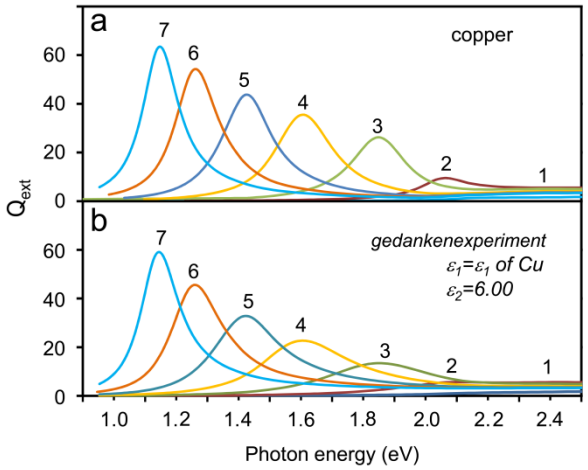

Figure A1. Effect of shape on the localized surface plasmon resonance in (a) Cu nanoparticles compared to (b) the hypothetical material of the *gedankenexperiment*. The aspect ratio of each nanorod is shown above its curve).

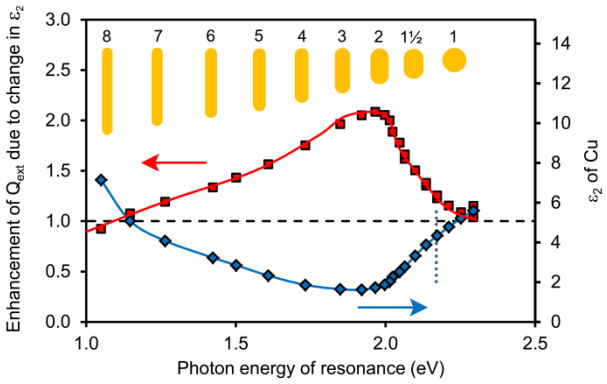

Figure A2. Enhancement of LPSRs in pure Cu (upper curve) due to dispersion of ε_2 with photon energy (lower curve). The position of Cu's absorption edge is shown as a dotted line segment. The aspect ratios (length/diameter) and silhouettes of the equivolume series of shapes are shown along the top of the figure.

[1] Dowd, A., Pissuwan, D. and Cortie, M. B. 2014 Optical readout of the intracellular environment using nanoparticle transducers *Trends in Biotech.* **32**(11) 571.
[2] Hill, R. T. 2015 Plasmonic biosensors *Wiley Interdisciplinary Reviews: Nanomedicine and Nanobiotechnology* **7**(2) 152.
[3] Ross, M. B., Blaber, M. G. and Schatz, G. C. 2014 Using nanoscale and mesoscale anisotropy to engineer the optical response of three-dimensional plasmonic metamaterials *Nature Comm.* **5** 4090.
[4] Cole, J. R. and Halas, N. J. 2006 Optimised plasmonic nanoparticle distributions for solar spectrum harvesting *Appl. Phys. Lett.* **89**(15) 153120.
[5] Stokes, N. L., Edgar, J. A., McDonagh, A. M. and Cortie, M. B. 2010 Spectrally selective coatings of gold nanorods on architectural glass *J. Nanopart. Res.* **12**(8) 2821
[6] Loo, C., Lowery, A., Halas, N., West, J. and Drezek, R. 2005 Immunotargeted Nanoshells for Integrated Cancer Imaging and Therapy *Nano Lett.* **5**(4) 709.
[7] Ayala-Orozco, C., Urban, C., Bishnoi, S., Urban, A., Charron, H., Mitchell, T., Shea, M., Nanda, S., Schiff, R., Halas, N. and Joshi, A. 2014 Sub-100 nm gold nanomatryoshkas improve photo-thermal therapy efficacy in large and highly aggressive triple negative breast tumors *J. Controlled Release* **191** 90.
[8] Blaber, M. G., Arnold, M. D., Harris, N., Ford, M. J. and Cortie, M. B. 2007 Plasmon absorption in nanospheres: A comparison of sodium, potassium, aluminium, silver and gold *Phys. B (Amsterdam, Neth.)* **394**(2) 184.
[9] Cortie, M., Xu, X. and Ford, M. 2006 Effect of composition and packing configuration on the dichroic optical properties of coinage metal nanorods *Phys. Chem. Chem. Phys.* **8** 3520.
[10] Guo, H., Chen, Y., Cortie, M. B., Liu, X., Xie, Q., Wang, X. and Peng, D.-L. 2014 Shape-selective formation of monodisperse copper nanospheres and nanocubes via disproportionation reaction route and their optical properties *J. Phys. Chem. C* **118**(18) 9801.
[11] Hymes, S., Murarka, S. P., Shepard, C. and Lanford, W. 1992 Passivation of copper by silicide formation in dilute silane *J. Appl. Phys.* **71**(9) 4623.
[12] Lanford, W. A., Ding, P. J., Wang, W., Hymes, S. and Muraka, S. P. 1995 Low-temperature passivation of copper by doping with Al or Mg *Thin Solid Films* **262**(1–2) 234.
[13] Ding, P. J., Wang, W., Lanford, W. A., Hymes, S. and Murarka, S. P. 1994 Thermal annealing of buried Al barrier layers to passivate the surface of copper films *Appl. Phys. Lett.* **65**(14) 1778.
[14] Fox, M. 2010 *Optical Properties of Solids*, (Oxford, U.K.: Oxford University Press).
[15] Blaber, M. G., Arnold, M. D. and Ford, M. J. 2009 Optical properties of intermetallic compounds from first principles calculations: a search for the ideal plasmonic material *J. Phys.: Condens. Matter* **21**(14) 144211.
[16] Arnold, M. D. and Blaber, M. G. 2009 Optical performance and metallic absorption in nanoplasmonic systems *Optics Express* **17**(5) 3835.
[17] Ehrenreich, H. and Philipp, H. R. 1962 Optical Properties of Ag and Cu *Phys. Rev.* **128**(4) 1622.
[18] Bobb, D. A., Zhu, G., Mayy, M., Gavrilenko, A. V., Mead, P., Gavrilenko, V. I. and Noginova, M. A. 2009 Engineering of low-loss metal for nanoplasmonic and metamaterials applications *Appl. Phys. Lett.* **95** 151102.
[19] Jellison, G. E. and Modine, F. A. 1996 Parameterization of the optical functions of amorphous materials in the interband region *Appl. Phys. Lett.* **69** 371.
[20] Jellison, G. E. and Modine, F. A. 1996 Erratum: ''Parameterization of the optical functions of amorphous materials in the interband region'' [Appl. Phys. Lett. 69, 371 (1996)] *Appl. Phys. Lett.* **69** 2137.
[21] Blaha, P., Schwarz, K., Madsen, G. K. H., Kvasnicka, D. and Luitz, J. 2001 *WIEN2k, An Augmented Plane Wave + Local Orbitals Program for Calculating Crystal Properties* (Vienna, Austria: Techn. Universität Wien).
[22] Perdew, J. P., Burke, K. and Ernzerhof, M. 1996 Generalized gradient approximation made simple *Physical Review Letters* **77** 3865.
[23] Ambrosch-Draxl, C. and Sofo, J. O. 2006 Linear optical properties of solids within the full-potential linearized augmented planewave method *Comp. Phys. Comm.* **175** 1.
[24] Vast, N., Reining, L., Olevano, V., Schattschneider, P. and Jouffrey, B. 2002 Local field effects in the electron energy loss spectra of rutile TiO_2 *Phys. Rev. Lett.* **88** 037601.
[25] Keast, V. J. 2013 An introduction to the calculation of valence EELS: Quantum mechanical methods for bulk solids *Micron* **44** 93.
[26] McPherson, D. J., Supansomboon, S., Zwan, B., Keast, V. J., Cortie, D. L., Gentle, A., Dowd, A. and Cortie, M. B. 2014 Strategies to control the spectral properties of Au-Ni thin films *Thin Solid Films* **551** 200.
[27] Keast, V. J., Birt, K., Koch, C. T., Supansomboon, S. and Cortie, M. B. 2011 The role of plasmons and interband transitions in the color of $AuAl_2$, $AuIn_2$ and $AuGa_2$ *Appl. Phys. Lett.* **99**(11) 111908.
[28] Pearson, W. B. 1958 *A Handbook of Metal Physics and Physical Metallurgy*, (Oxford: Pergamon Press).
[29] Kuwano, N., Ogata, I. and Eguchi, T. 1975 Effect of short range order on lattice parameter in alpha phase of Cu-Al *J. Japn. Inst. Metals* **39**(6) 609.
[30] De Silva, K. S. B., Gentle, A., Arnold, M., Keast, V. J. and Cortie, M. B. 2015 Dielectric function and localized plasmon resonances of equiatomic Au-Cu *J. Phys. D: Appl. Phys.* **48** 215304.
[31] Marini, A., Onida, G. and DelSole, R. 2002 Quasiparticle electronic structure of copper in the GW approximation *Phys. Rev. Lett.* **88** 016403.
[32] Marini, A., DelSole, R. and Onida, G. 2002 First-principles calculation of the plasmon resonance and of the reflectance spectrum of silver in the GW approximation *Phys. Rev. B* **66** 115101.
[33] Alkauskas, A., Schneider, S. D., Hébert, C., Sagmeister, S. and Draxl, C. 2013 Dynamic structure factors of Cu, Ag, and Au: Comparative study from first principles *Phys. Rev. B* **88** 195124.
[34] *Materials and methods are available as supplementary materials on Science Online*.
[35] Draine, B. T. and Flatau, P. J. 1994 Discrete-dipole approximation for scattering calculations *J. Opt. Soc. Am. A* **11**(4) 1491.

[36] Murray, J. L. 2002 *Alloy Phase Diagrams*, Vol. 3 (Materials Park, Ohio: ASM Materials International).
[37] Rosei, R., Modesti, S., Prantera, V. and Davoli, I. 1979 Shift of electronic states at L in α-phase Cu-Zn and Cu-Al alloys *J. Phys. F: Metal Physics* **9**(11) 2275.
[38] Rao, R. S., Prasad, R. and Bansil, A. 1983 Composition dependence of optical gaps in copper-based Hume-Rothery alloys *Phys. Rev. B* **28**(10) 5762.
[39] Rea, R. S. and DeReggi, A. S. 1974 Interband optical properties and electronic structure of α-phase disordered copper-aluminum alloys *Phys. Rev. B* **9**(8) 3285.
[40] Carotenuto, C., Rosei, R. and Sommacal, M. 1976 Interband absorption edge shift in dilute α-phase Cu-Zn and Cu-Al alloys *Solid State Comm.* **19**(6) 547.
[41] Wang, H., Tam, F., Grady, N. K. and Halas, N. J. 2005 Cu nanoshells: effects of interband transitions on the nanoparticle plasmon resonance *J. Phys. Chem. B* **109** 18218.
[42] Salzemann, C., Brioude, A. and Pileni, M.-P. 2006 Tuning of copper nanocrystals optical properties with their shapes *J. Phys. Chem. B* **110** 7208.
[43] Liu, Z., Yang, Y., Liang, J., Hu, Z., Li, S., Peng, S. and Qian, Y. 2003 Synthesis of copper nanowires via a complex-surfactant-assisted hydrothermal reduction process *J. Phys. Chem. B.* **107** 12658.
[44] Sekhon, J. S. and Verma, S. S. 2012 Rational selection of nanorod plasmons: material, size, and shape dependence mechanism for optical sensors *Plasmonics* **7** 453.